Environmental Science
Processes & Impacts

Accepted Manuscript

ROYAL SOCIETY OF CHEMISTRY

rsc.li/process-impacts

Table of Contents Entry

The long-lived fission product ^{79}Se is tightly bound to the UO_2 lattice in spent nuclear fuel; it will thus be released only very slowly from a geological repository for radioactive waste.

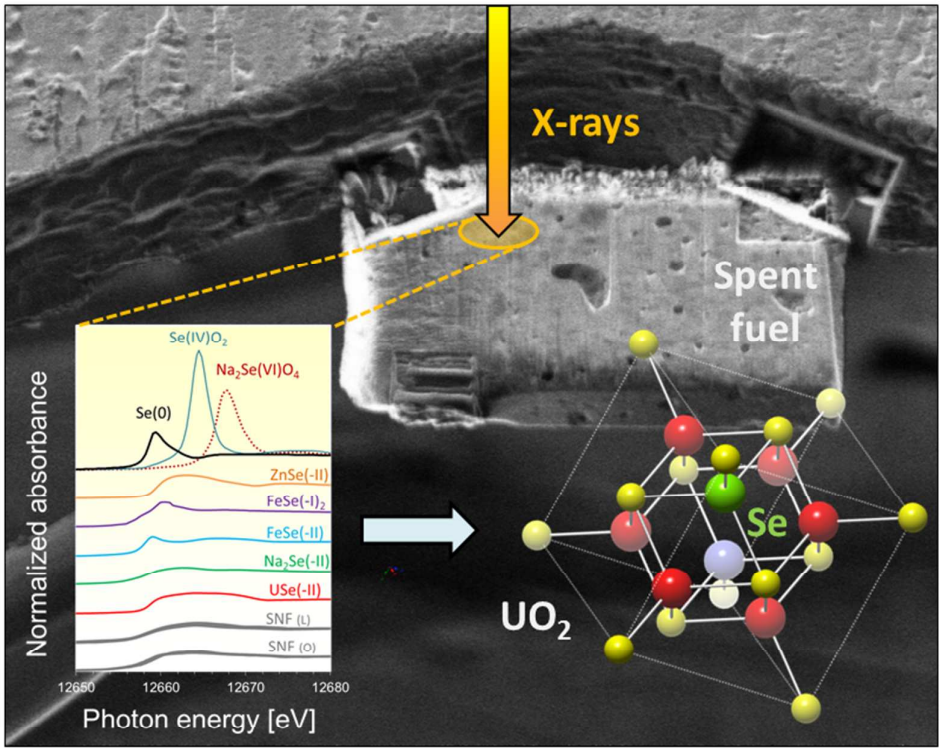

Environmental impact

The long-lived fission product ^{79}Se is a relevant nuclide in risk assessments of radioactive waste repositories. In the absence of reliable data and sufficient process understanding, it was previously assumed that a significant part of the ^{79}Se inventory is rapidly released from the spent fuel waste on contact with aqueous solutions, resulting in major contributions to the overall calculated radiological dose. Our spectroscopic data and thermodynamic calculations indicate that most of the selenium is tightly bound as sparingly soluble selenide ion in the crystalline lattice of UO_2 matrix, thus providing a mechanistic explanation for the low selenium release rates recently measured in aqueous leaching experiments. These results suggest that lower rates of fast release should be assumed for ^{79}Se in future safety assessments.

Environmental Science: Processes & Impacts

ARTICLE

Characterization of selenium in UO_2 spent nuclear fuel by micro X-ray absorption spectroscopy and its thermodynamic stability

Received 00th January 20xx,
Accepted 00th January 20xx

DOI: 10.1039/x0xx00000x

www.rsc.org/

E. Curti*[a], A. Puranen[b], D. Grolimund[a], D. Jädernas[b], D. Sheptyakov[a] and A. Mesbah[c,d]

Direct disposal of spent nuclear fuel (SNF) in deep geological formations is the preferred option for the final storage of nuclear waste in many countries. In order to assess to which extent radionuclides could be released to the environment, it is of great importance to understand how they are chemically bound in the waste matrix. This is particularly important for long-lived radionuclides such as ^{79}Se, ^{129}I, ^{14}C or ^{36}Cl, which form poorly sorbing anionic species in water and therefore migrate without significant retardation through argillaceous repository materials and host rocks. We present here X-ray absorption spectroscopic data providing evidence that in the investigated SNF samples selenium is directly bound to U atoms as Se(-II) (selenide) ion, probably replacing oxygen in the cubic UO_2 lattice. This result is corroborated by a simple thermodynamic analysis, showing that selenide is the stable form of Se under reactor operation conditions. Because selenide is almost insoluble in water, our data indirectly explain the unexpectedly low release of Se in short-term aqueous leaching experiments, compared to iodine or cesium. These results have a direct impact on safety analyses for potential nuclear waste repository sites, as they justify assuming a small fractional release of selenium in performance assessment calculations.

1. Introduction

In the past years, several nuclear energy producing countries have decided to abandon fuel reprocessing due to weapon proliferation issues, or due to the renouncement of a closed fuel cycle policy. As a result, direct disposal of spent nuclear fuel (SNF) in deep underground repositories has become an option for the final storage of high-level radioactive waste from nuclear power plants[1]. Safety assessments for such nuclear waste repository sites must therefore provide reliable long-term predictions on the release of radionuclides from SNF as the waste undergoes corrosion by ground water.

During reactor operation, severe microstructural and chemical changes take place in the fuel due to the high thermal stress as well as fission and decay processes. As a consequence, SNF is a highly heterogeneous material consisting of fuel matrix (essentially crystalline UO_2 or a UO_2-PuO_2 mixture) with 3%-6% fission products and minor actinides dispersed among different phases. Minor actinides such as Am, Cm and Np typically form solid solutions by replacing U(IV) and Pu(IV) in the primary U, Pu oxide lattice, whereas the fission products Mo, Tc, Ru, Pd and sometimes Te are concentrated in newly formed metallic phases (the so-called ε-particles). Gaseous elements (He, Kr, Xe) rapidly diffuse towards grain boundaries and form intra- and intergranular gas bubbles or escape into the thin gap between fuel pellet and cladding. Volatile fission/activation products like I, Cs and Cl have also a tendency to segregate out of the fuel matrix and tend to follow the fission gas. Consequently, they are enriched at grain boundaries and in the fuel-cladding gap. Moreover, these elements are easily soluble in water at all oxidation potentials and sorb only weakly on mineral surfaces, implying that – once dissolved – under repository conditions they will migrate without significant retardation through engineered barriers and host rock. Therefore, it is not surprising that long-lived radionuclides such as ^{135}Cs, ^{129}I and ^{36}Cl are major contributors to the overall radiological dose calculated in safety analyses of nuclear waste repositories.

Radionuclide release from SNF in a deep water-saturated repository normally proceeds via two parallel mechanisms: (a) a short-term release of easily accessible soluble radionuclides (e.g. ^{129}I, ^{135}Cs, ^{36}Cl) over the first weeks to months after contact with ground water ("Instant Release Fraction", shortly IRF); (b) the much slower release through dissolution of the UO_2 or PuO_2 lattice ("matrix dissolution", MD) and other minor phases. In a repository, matrix dissolution is essentially an electrochemical process governed by the interplay of oxidants produced via water radiolysis and reactive molecular hydrogen[2,3,4] supplied by the corrosion of metallic waste containment. There is now a widespread consensus that H_2 produced by the anaerobic aqueous corrosion of such metallic (steel, copper) canisters will react with the peroxide and other oxidants produced by water radiolysis thanks to the catalytic effect of ε-particles[5,6,7]. This process prevents oxidation of

[a] Paul Scherrer Institut, 5232 Villigen PSI, Switzerland. E-Mail: enzo.curti@psi.ch
[b] Studsvik Nuclear AB, Nyköping, Sweden
[c] Department of Chemistry, Northwestern University, 2145 Sheridan Road, Evanston, IL 60208-3113, U.S.
[d] ICSM UMR 5257 CNRS/CEA/UM2/ENCSM, Site de Marcoule – Bât 426, BP 17171, 30207 Bagnols-sur-Cèze, France

$U(IV)O_2$ or $Pu(IV)O_2$ to more soluble U(VI) and Pu(VI) oxides, ensuring that the release of radionuclides will proceed at low fractional rates in the order of 10^{-6} to 10^{-7} per day[8].

The safety of planned underground repositories for radioactive waste worldwide largely relies on in-depth understanding of geochemical processes involved in the release, chemical reactions and transport of radionuclides from the waste to the biosphere. Insufficient knowledge of specific processes is usually compensated by conservatism in the choice of parameters for safety assessment calculations. A typical example is the IRF, which is poorly known for specific long-lived nuclides, e.g. ^{79}Se, due to the technical difficulty of obtaining sound experimental data on such highly radioactive materials.

The determination of nuclide-specific IRF-values has been and is still the subject of intensive studies[3,9]. IRF-values can be roughly estimated from reactor operational parameters such as linear power rate, fuel burn-up and measurements of fission gas release. However, the type of fuel, as well as contributions of activation products from different material sources (e.g. ^{14}C from Zircaloy), may also play a major role. UO_2 fuels with burnup exceeding 40 GWd/tU, like those investigated in the present study, also develop a peripheral region about 100 μm thick, called "rim", characterized by higher fission product concentrations, nanometric grain size and higher porosity compared to the bulk of the pellet. The formation of the "rim" is induced by the higher fission probability at the pellet boundary, which increases defect formation and, thus, induces restructuring of the fuel. Due to the higher porosity and increased fission product concentrations, the "rim" was previously regarded as a preferential source of IRF nuclides. However, leaching data not always support this view[9] and there is increasing evidence that the rim may even have a protective effect against fast radionuclide release[10,11,12]. In summary, for each nuclide of interest the IRF (understood as the sum of the short-term release from fuel grain boundaries, fuel/cladding gap and Zircaloy cladding corrosion layers) is a critical, but still poorly known safety-assessment parameter, resulting from a variety of material properties and in-reactor processes.

The present contribution focuses on ^{79}Se, a long-lived nuclide (half-life 3.3×10^5 a) traditionally considered as a significant IRF contributor, owing to the appreciable volatility of selenium under reactor operation conditions (boiling point: 685 °C at 1 bar) and the high solubility of oxidized Se species in water[13,14]. According to this view, during reactor operation a significant fraction of the Se inventory would segregate as Se(0) towards grain boundaries and the fuel/cladding gap. Radiolytic oxidants would then oxidize it to easily leachable Se(IV) or Se(VI) on contact with ground water. Accordingly, IRF values of up to 17% have been proposed conservatively for safety assessment analyses of spent fuel repository sites[15]. However, so far SNF leaching data do not support this figure and point to very low IRF values for ^{79}Se[9]. Moreover, experimental data on the chemical state of selenium in UO_2 spent fuel are very scarce.

The present study aims at increasing the knowledge on the chemical state of selenium in SNF and finalizes a previously published work[16]. In that study, X-ray Absorption Near Edge Spectroscopy (XANES) measurements on high-burnup SNF micro-particles from the Leibstadt boiling water reactor (Switzerland) suggested that Se occurs in those samples as reduced Se(-II) (selenide), which unlike Se(IV)/Se(VI) is almost insoluble in water[13,14] and, therefore, has limited mobility. The evidence was, however, indirect and inconclusive, as it was provided via theoretical calculations of XANES spectra. A direct comparison with experimental spectra of reference U-Se compounds was not possible in that investigation. In the present study, we provide supplemental XANES data on SNF from the Oskarshamn-III boiling water reactor and new XANES spectra from two well-characterized crystalline U-selenide reference compounds (α-USe_2 and USe) allowing a direct comparison (fingerprinting) with the SNF spectra and, thus, more robust conclusions on the nature of Se fission products in high-burnup UO_2 SNF. In addition, we attempt to correlate the spectroscopic data with the results of thermodynamic stability calculations in the system U-Se-O.

2. Experimental methods and data evaluation

2.1 Sample Preparation

A total of six samples were prepared for X-ray spectroscopy from two SNF pellets, one originating from Leibstadt (Switzerland) and one from Oskarshamn-III (Sweden), both boiling water reactors. Due to radiation protection limitations, only micro-samples could be studied, implying challenging preparation techniques. The Leibstadt fuel was unloaded in August 2004 after 9 burning cycles and has a burnup of 78.7 GWd/tU. It was prepared by collecting dispersed SNF particles on Kapton tape after gentle abrasion of the pellet surface, taking care to preserve their radial position[16]. The Oskarshamn-III samples were prepared by Focused Ion Beam (FIB) milling at Studsvik Nuclear AB, using a Zeiss® equipment with a Ga ion source. They originate from a "matchstick"-sized fuel strip (average burn-up 62.9 GWd/tU) encompassing the entire pellet diameter (from clad to clad) and passing through the center. Two polished microsamples of approximately (L x W x H) = (30 x 15 x 5) μm^3 were produced: (a) the "RIM" sample from the pellet periphery, including the outer boundary of the pellet, i.e. the fuel-gap interface (Fig. 1); (b) the "CEN" sample from the center of the pellet. The RIM sample was brought with a special tip onto an Omniprobe® Lift-Out Grid, using a carbon source as welding material (instead of Pt) to avoid interferences with the emission spectra of selenium during fluorescence detection. The CEN sample detached unintentionally from the grid during preparation, but it could be recovered and fixed with a strip of Kapton tape.

Reference compounds for X-ray absorption spectroscopy were either purchased (Se(0), SeO_2, Na_2SeO_4, ZnSe, FeSe), obtained by chemical synthesis in specialized laboratories (Na_2Se, USe, α-USe_2) or prepared from natural mineral specimens ($FeSe_2$).

The synthesis of U-selenide compounds deserves special attention due to their critical role for the interpretation of our results. The USe sample is a NaCl-type cubic compound that was synthesized about 15 years ago for different purposes[17]. The synthesis was carried out under strictly reducing conditions, by reacting 20-μm thick turnings of U metal and a stoichiometric amount of Se metal in evacuated sealed quartz tubes at 600-800 °C over a period of 2-3 weeks[18]. XRD analyses carried out shortly before the X-ray absorption measurements indicated that the USe compound had undergone minor changes during the 15 years storage time in air. Specifically, formation of small amounts of U_3Se_4 was ascertained (see supplementary information). Since both USe and U_3Se_4 are pure Se(-II) compounds, this sample can still be considered as an appropriate XANES reference to probe selenide-uranium bonding environments. The α-USe_2 sample was synthesized specifically for this investigation at Northwestern University, following a technique described elswhere[19]. XRD examination (see supplementary information) revealed the presence of small amounts of metallic Se(0) at the time of the X-ray absorption measurements, possibly formed during transport and storage. This compound is therefore not a pure Se(-II) reference and could not be used directly for our data interpretation.

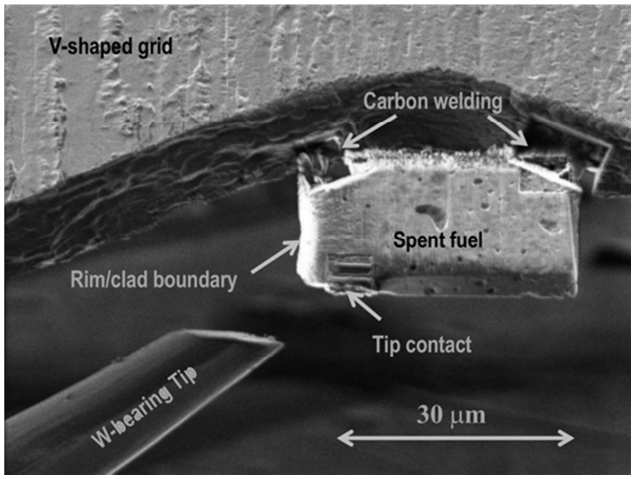

Fig. 1 FIB Sample ("RIM") of Oskarshamn-III spent fuel used for micro-XANES measurements (courtesy Studsvik Nuclear AB).

2.2 X-ray spectroscopy

All X-ray absorption (XAS) and X-ray fluorescence (XRF) measurements on SNF and on reference compounds were carried out at the microXAS beamline, Swiss Light Source (SLS), using a micro-focused, about 5 μm (horizontal) x 3 μm (vertical) monochromatic X-ray beam. The fluorescence signal was collected at photon energies of 12.6-13.2 keV (Se-K edge, Se mapping) and 17.3 keV (U mapping) using a single element Si detector (Ketek®), while the transmitted signal was recorded with a photodiode or an ionization chamber. The ionization chamber was 30 cm long and filled with N_2, resulting in a calculated absorption of about 7%. Thanks to the very intense beam delivered at SLS, even such a low percentage is sufficient to provide a stable and reliable absorption signal. Moreover, potential saturation effects are avoided. The absorption spectra of Se reference compounds were measured simultaneously in fluorescence and transmission. Photon energy calibration was carried out using a Se(0) reference.

Micro-XRF maps of the Se-K_α signal were obtained by scanning the sample surface with the micro-focused X-ray beam at the fixed photon energy of 12.7 keV, while collecting "on the fly" the emitted fluorescence intensity. In order to improve the spatial resolution of XRF maps, the beam size was reduced for this purpose to 3 μm (horizontal) x 1 μm (vertical) by partially closing two perpendicular slits in the beam path.

Reduction and evaluation of the X-ray absorption near-edge structure (XANES) and extended X-ray absorption fine structure (EXAFS) data were carried out using the ATHENA/ARTEMIS package[20]. Due to the unfavourable signal/noise ratio of the spectra collected on Leibstadt spent fuel, the in-built ATHENA interpolative smoothing procedure was applied to allow comparison with the spectra of reference compounds. A careful analysis showed that the edge and white line positions are not affected by the smoothing procedure.

During EXAFS data collection, the fluorescence signal was stable over several hours and successive scans did not show any alteration or energy shift in the collected absorption spectra. The effects of sample movements were minimized by opening the slits to a beam size of 5 μm x 3 μm.

3. X-ray spectroscopy

3.1 X-ray fluorescence

Fig. 2 shows the SeK_α fluorescence maps of the two FIB samples. The maps reveal a spatially homogeneous Se distribution throughout both samples, as detector counts vary within a factor of 2-3 in each sample‡. Low Se concentrations, in the order of 100 ppm, are expected in UO_2 SNF because of the low fission yield of Se isotopes by thermal neutrons. This led unavoidably to low SeK_α signal/noise ratios in the investigated SNF samples (Fig. 3). On the other hand, the fact that significant Se fluorescence was measurable over the entire sample surfaces provides convincing evidence that most of the Se inventory generated during the fission reactions still resides in the SNF, i.e. one can exclude segregation of a major fraction of the Se inventory into the fuel/cladding gap. This information is important as it indicates a limited mobility of Se in spite of the high burnup of the fuel.

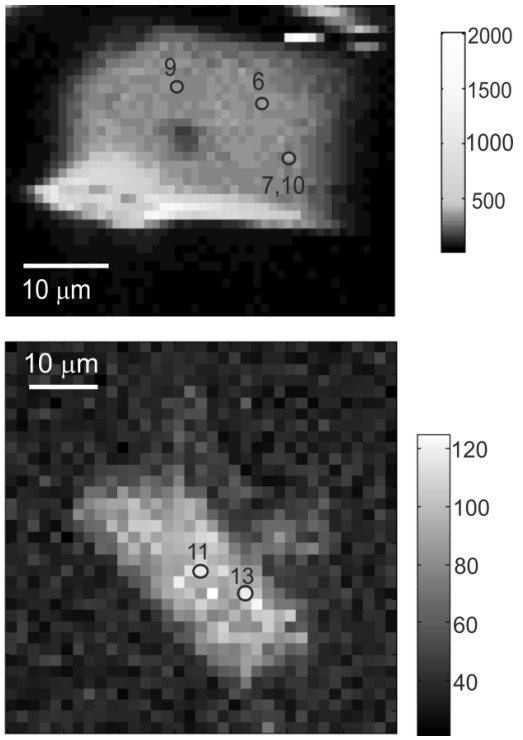

Fig. 2 Micro-XRF maps showing the Se-K_α intensities of RIM (top) and CEN (bottom) spent fuel samples. The bars indicate detector counts.

Fig. 3 shows the fluorescence spectra collected at four distinct pixel locations on the CEN and RIM samples, with identification of the Se, Nd and Ga peaks. The dominating Ga signal is the result of implantation during FIB preparation. From the fluorescence spectra, we were able to obtain semi-quantitative information on the distribution of Se within the pellet. By normalizing the Se and Nd signals to the Ga signal (assuming comparable Ga implantation in the two samples), we could assess that both Nd and Se are significantly enriched in the rim region, since the SeK_α/GaK_α and NdL_α/GaK_α signal ratios are significantly higher in the RIM sample compared to the CEN sample. This is in agreement with the expected increased local burnup of the rim structure. There is, however, no evidence for preferential segregation of Se with respect to matrix-compatible elements, since the SeK_α(RIM)/SeK_α(CEN) and NdL_α(RIM) /NdL_α(CEN) ratios were found to be similar (about 10).

3.2 XANES experiments

Fig. 4 is a stacked diagram illustrating the Se K-edge XANES spectra obtained from the SNF samples in comparison with experimental spectra of Se reference compounds. The SNF spectra (bottom, in grey) appear as thickened lines since they are in fact envelopes resulting from about 30 single micro-XANES measurements collected at different locations on six SNF samples (two from Oskarshamn-III and four from Leibstadt). All SNF spectra proved to be very similar, independently of reactor origin. This finding is central for this study, since it indicates that Se occurs in all investigated SNF samples in a characteristic chemical state.

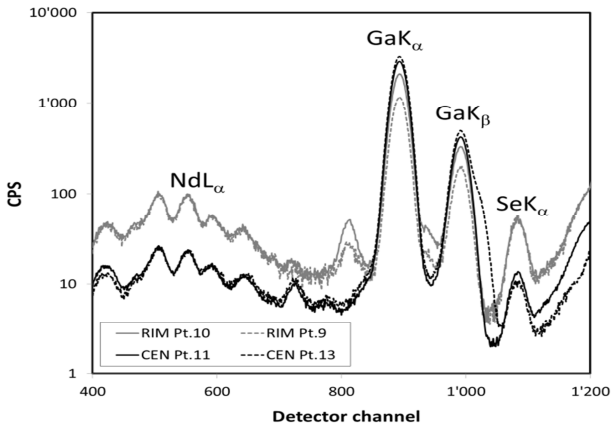

Fig. 3 Fluorescence spectra recorded at four different locations of the Oskarshamn-III SNF samples.

The spectra of Se(0) (grey selenium), $Se(IV)O_2$ and $Na_2Se(VI)O_4$ are characterized by prominent white lines, which are strongly depressed or absent in the Se(-I,-II) compounds. By comparison of the spectra, one can rule out Se to occur in the SNF samples as pure forms of either Se(0), Se(IV) or Se(VI). A combination of about 50% Se(0) and 50% Se(IV) is theoretically possible but very unlikely, since it would imply that the same mixture would occur in exactly the same proportion in all samples (see discussion in our previous publication)[16]. The SNF spectra have striking similarities to the spectra of Se(-II) (selenide) compounds, which have a depressed white line or lack it completely. The absence of a prominent white line in selenide compounds is due to the full occupancy of p-orbitals in this reduced form of selenium.

By far the best match with the SNF spectra is found for USe(-II), suggesting a direct binding of Se(-II) to U atoms in the SNF samples. The similarity between SNF and USe(-II) XANES is evidenced by Fig. 5, where the normalized spectra obtained on USe(-II) in fluorescence and transmission are directly superposed to the averaged[§] XANES of the SNF samples on an enlarged scale. Considering the relatively low signal/noise ratio in the SNF data, the small differences between Leibstadt and Oskarshamn-III spectra are probably not significant. Thus, the close similarity of the two sets of spectra likely indicates a comparable chemical environment of Se in the fuels of the two reactors.

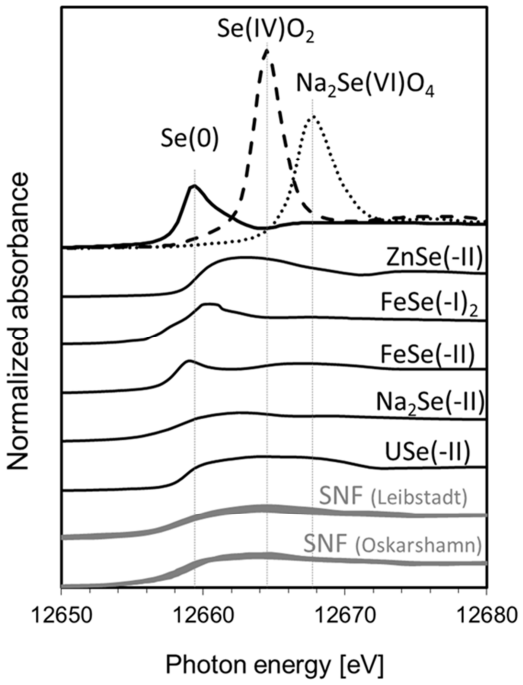

Fig. 4 XANES spectra obtained from SNF samples and Se reference compounds.

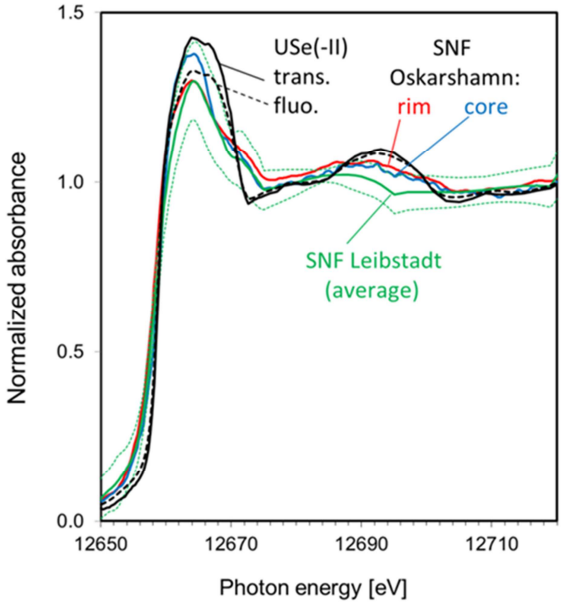

Fig. 5 Superposition of XANES spectra obtained on USe(-II) and SNF averaged spectra. The dotted green lines delimit the envelope of all data from Leibstadt fuel.

3.3 Ab initio XANES

Ab initio Se K-edge XANES spectra of the USe and α-USe_2 crystal structures were calculated using the FDMNES program[21]. The crystallographic data were derived from entries 68418 and 57186 of the ICSD database[22]. The calculations were performed on small spherical clusters (3 Å radius) around a central Se absorber, assuming an amplitude reduction factor (S_0^2) of 1.0, Green formalism (multiple scattering) on a muffin-tin potential and self-consistent potentials. The aim was to provide theoretical standards for the two U-Se compounds, in addition to the experimental spectra. This was particularly useful to generate a reference spectrum for α-USe_2, as the measured spectrum could not be used directly as experimental standard due to contamination of the sample with Se(0) (see XRD data in the supplementary information). Moreover, the comparison of *ab initio* and experimental spectra serves as a consistency check. Fig. 6 shows the *ab initio* and corresponding experimental spectra collected on the USe and α-USe_2 samples, compared to a characteristic spectrum measured on SNF from the Leibstadt reactor.

Inspection of Fig. 6 shows that, despite small differences between the theoretical spectra of the USe and the α-USe_2, the two theoretical reference spectra are very similar and match fairly well the SNF spectrum. The theoretical α-USe_2 XANES seems to reproduce the SNF spectrum even better. In summary, the ab initio calculations support the former conclusion (arising from the comparison with the experimental reference spectra) that Se occurs as selenide directly bound to U atoms in the studied SNF samples. The marked difference between experimental and theoretical α-USe_2 spectra (white line in the experimental spectrum) confirms the contamination of this reference compound by metallic selenium, evidenced by the XRD data.

3.4 Structural considerations

Fig. 7 shows the coordination geometries around Se atoms in USe and α-USe_2. In the former compound, which has cubic NaCl-type symmetry, Se(-II) ions have an undistorted octahedral coordination, whereas α-USe_2 has four distinct Se sites with distorted tetrahedral coordination. Thus, there are large differences in the coordination environments of USe and α-USe_2, the former having six, the second only four U neighbours. Moreover, although the oxidation state of Se is the same in both compounds (-II), the oxidation state of U is different (+II and +IV, respectively). In spite of such differences the theoretical XANES spectra of the two compounds are similar, suggesting that the Se-K XANES of Se(-II)-U bonding environments is quite insensitive to the coordination geometry and number/valence of surrounding U atoms. Therefore, it appears that these spectra are a characteristic geometry-independent XANES signature of U-Se(-II) bonds.

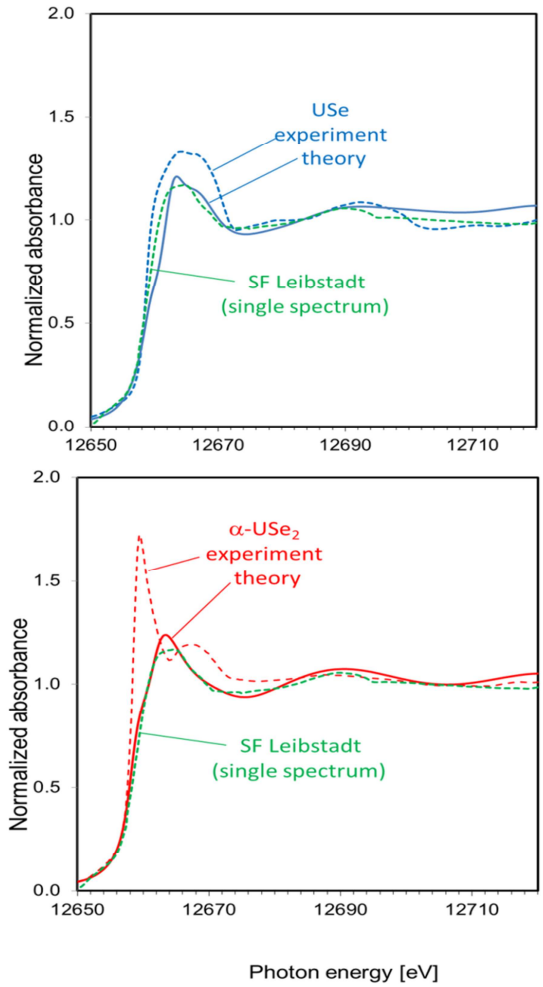

Fig. 6 Superposition of theoretical and experimental spectra for USe (top) and α-USe_2 (bottom) compared to a typical single spectrum collected on Leibstadt SNF.

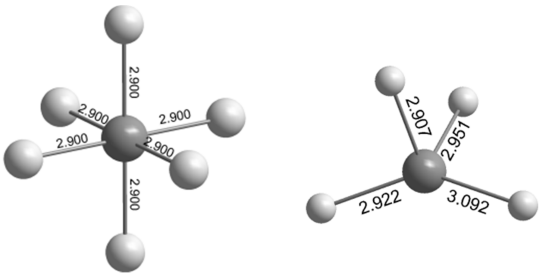

Fig. 7 Coordination spheres of Se (dark grey) in USe (left) and in a specific site of α-USe_2 (right). Light grey spheres represent U atoms, numbers denote distances in Å, specified from XRD data.

In our previous study[16], it was postulated that Se(-II) replaces oxygen positions in the lattice of the UO_2 matrix. We were able to reproduce the XANES spectra obtained on Leibstadt SNF by ab initio XANES calculations coupled with a geometric optimization procedure, which showed that XANES spectral features are sensitive to Se-U interatomic distances. A best fit coordination was determined for Se-U distances of 2.87 ± 0.03 Å. This fit is consistent with available XRD data, since a search in the ICSD database[22] showed that Se-U interatomic distances in U-Se(-II) compounds lie within a restricted range, with a strong frequency maximum between 2.85 Å and 2.95 Å. This result together with the agreement between SNF and U-Se(-II) XANES spectra found in the present study provide strong arguments in favour of the proposed Se(-II) for O(-II) substitution in the UO_2 lattice.

3.5 Extended X-ray absorption fine structure (EXAFS)

Due to the very small Se concentrations in SNF (in the order of 100 ppm), the heavy UO_2 matrix, and the microscopic nature of the samples, full EXAFS measurements allowing independent determination of interatomic distances and coordination were precluded. This was also the main reason for focusing on XANES in this study. Nevertheless, the Oskarshamn-III samples yielded a better fluorescence signal compared with the previously studied Leibstadt SNF[16]. This is ascribed to the better quality of the Oskarshamn-III samples, as the FIB preparation yielded a flat surface and a larger sample thickness. In two locations of the RIM sample the signal quality was judged to be sufficiently good to attempt measurements over the EXAFS region. The results of one of two (equivalent) EXAFS measurements are illustrated in Table 1 and Fig. 8.

As expected, the signal allowed analysis only to a limited wave vector range. Beyond k = 6 $Å^{-1}$ the background noise was exceedingly high, precluding the identification of further oscillations. Despite these limitations, we attempted a data analysis. As in the *ab initio* XANES calculations carried out in the previous study[16], we assumed replacement of oxygen atoms by isolated Se atoms in the UO_2 lattice. A single-scattering model including two shells (Se-U, Se-O) was refined after fixing the coordination numbers, from which Se-U distances could be fitted with reasonable precision (2.88 ± 0.05 Å). This agrees fairly well with the Se-U distances determined by geometric optimization of the XANES spectra in the former study[16] (2.87 ± 0.03 Å). In contrast, Se-O distances could not be determined precisely. Note also that the fitted Debye-Waller factors (σ^2) are also unusually large. Nevertheless, the 1-shell fit involving only Se-U pairs was definitely less successful than the 2-shell fit, yielding higher R-factor (0.096) and reduced χ^2 values (226.8).

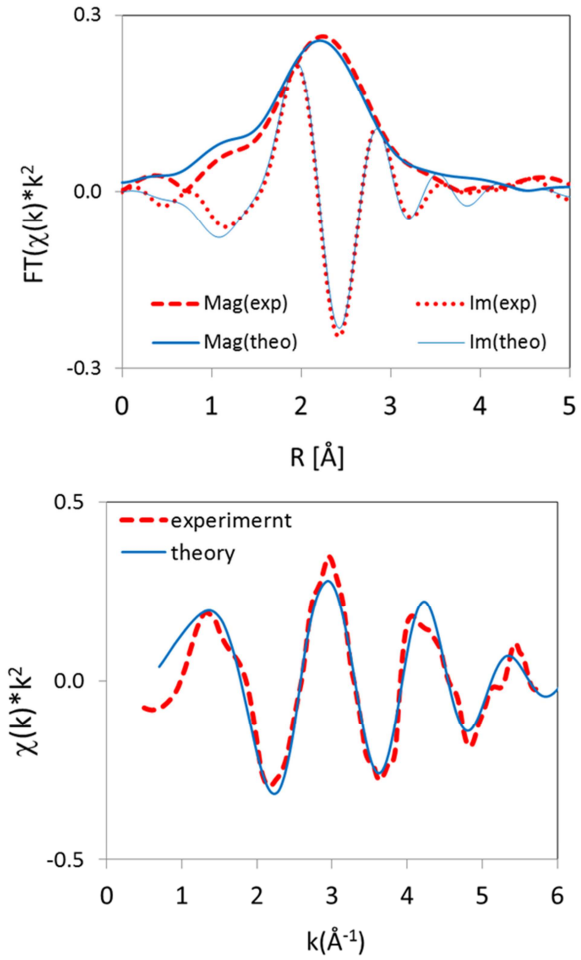

Fig. 8 EXAFS fit results for a specific location (Pt. 6) of the Oskarshamn-III RIM sample carried out in R-space between k= 0.5 Å^{-1} and k=5 Å^{-1} over the R range 1-4 Å. Top: Magnitude and imaginary parts of fitted spectrum (blue) and experimental spectrum (red) in R-space. Bottom: Experimental spectrum and back-transformation in k-space.

Table 1 EXAFS fit results for a specific location (Pt. 6) of the Oskarshamn-III RIM sample. Parameters in *italics* were fixed during the fitting procedure. The S_0^2 value was calculated using electron shake-off probabilities[23]. The R-factor and reduced χ^2 calculated with ARTEMIS[20] were 0.018 and 70.8, respectively.

Se-U			Se-O				
CN	R (Å)	σ^2 (Å^2)	CN	R (Å)	σ^2 (Å^2)	ΔE_0 (eV)	S_0^2
4	2.88 ± 0.05	0.029 ± 0.014	*6*	2.98 ± 0.14	0.042 ± 0.031	1.64 ± 3.05	*0.91*

4. Thermodynamic calculations

Simple thermodynamic calculations were carried out to determine the stability boundaries between USe_2/Se(cr), Se(cr)/SeO_2 and SeO_2/SeO_3, using state-of-the-art thermodynamic data. The results are reported in a classical Ellingham diagram (Fig. 9), in which the partial molar free energy of formation of oxides from their metals ($\Delta\bar{G}_{O_2} = RTln\,(pO_2)$, the oxygen potential) is plotted as a function of temperature for each pair. Such diagrams are routinely used as a first mean to evaluate the chemical state of fission products in SNF under reactor operation and dry storage conditions. This is done by comparing the oxygen potential of a given fission product (FP) with the oxygen potential of the fuel. Whenever $\Delta\bar{G}_{O_2}$(FP) > $\Delta\bar{G}_{O_2}$(fuel) the fission product should be stable in its reduced form and appear in the metallic state (e.g. Pd(0) in the so-called ε-particles). Conversely, if $\Delta\bar{G}_{O_2}$(FP) < $\Delta\bar{G}_{O_2}$(fuel) the fission product should appear in a separate oxide phase.

The determination of the fuel oxygen potential, even for pure UO_2 fuel, is not a trivial task as it depends in a complex way on UO_2 hyper-stoichiometry, the concentration of FPs and actinides in the UO_2 lattice and on the ability of incompatible FPs to buffer the oxygen potential[24,25,26]. Cordfunke and Konings[26] were able to restrain $\Delta\bar{G}_{O_2}$ for light water reactor (LWR) UO_2 fuels to a range between -550 and -450 kJ/mol, which we will use for the comparison with the oxygen potential calculations of Se species presented below.

Although oxygen potential calculations are available for most common fission products, they cannot be found for selenium. This may partly be due to the low fission yield of Se isotopes, which, thus, has little impact on the oxygen budget of the fuel, or to the limited availability of reliable thermodynamic data in earlier times. More likely, the lack of oxygen potential calculations for Se is related to the fact that only recently has ^{79}Se been identified as a potentially dose-determining nuclide in safety assessment calculations for radioactive waste repositories.

In order to evaluate the stability of Se oxidation states (-II, 0, IV, VI) in spent UO_2 fuel (both at reactor operation and storage temperatures), the following equilibria have been assessed:

$USe_2(cr) + O_2(g) = UO_2(cr) + 2\,Se(cr)$ (I)

$Se(cr) + O_2(g) = SeO_2\,(cr)$ (II)

$SeO_2(cr) + ½\,O_2(g) = SeO_3\,(cr)$ (III)

Since all solids are assumed to be pure, the equilibrium state for each of the above reactions at constant pressure and temperature will be defined by a fixed oxygen partial pressure (pO_2). This is related to the oxygen potential by the simple relation $\Delta\bar{G}_{O_2} = RTln\,(pO_2)$, where R is the gas constant (J K^{-1}

mol^{-1}) and T is absolute temperature (K). The standard molar Gibbs free energies of reaction ($\Delta_r G_m^o$ at 298.15 K, 1 bar) were calculated for reactions (I, II, III) by applying the following equations:

$$\Delta_r G_m^o = \sum_{prod} \Delta_f G_m^o - \sum_{reac} \Delta_f G_m^o$$

$$\Delta_f G_m^o = \Delta_f H_m^o - T\, S_m^o$$

where the summation symbols refer to products and reactants of the reaction, $\Delta_f G_m^o$ and $\Delta_f H_m^o$ are the standard molar free energy and enthalpy of formation, respectively (J mol^{-1}) and S_m^o is the absolute molar entropy (J mol^{-1} K^{-1}). Heat capacity values were extrapolated to higher temperatures by means of 5-term polynomials:

$c_{p,m}(T) = a + bT + cT^2 + \frac{d}{T} + \frac{e}{T^2}$ for all phases except O_2(g)

$c_{p,m}(T) = a + bt + ct^2 + ct^3 + \frac{e}{t^2}$c for O_2(g), where $t = T/1000$

The selected free energies, enthalpies and heat capacity coefficients are shown Table 2, which also reports the lower and higher limits of validity (T_{min}, T_{max}) of the heat capacity extrapolation. At T>T_{max}, the heat capacities were simply kept constant at $c_p(T_{max})$.

Table 2 Thermodynamic data used for the calculations depicted in Fig. 9.

		Se(cr)	α-USe_2	SeO_2	SeO_3	UO_2	O_2(g)	
Reference		**27**	**28**	**27**	**27**	**28**	**29**	
$\Delta_f G_m^o$	J mol^{-1}	0	-4.27E+5	-1.72E+5	-8.62E+4	-1.03E+6	0	
$\Delta_f H_m^o$	J mol^{-1}	0	-4.27E+5	-2.25E+5	-1.63E+5	-1.09E+6	0	
S_m^o	JK^{-1} mol^{-1}	42.09	134.98	67.49	91.74	77.03	205.15	
a		24.801	79.693	69.5	17.64	62.774	31.322	30.032
b		1.29E-3	8.65E-3	3.89E-3	2.00E-1	3.17E-02	-20.235	8.77
c		9.93E-6	0	0	0	0	57.866	-3.988
d		0	0	0	0	0	-36.506	0.788
e		-8.71E+4	-2.65E+5	-1.11E+6	0	-7.69E+5	-7.37E-3	-7.42E-1
T_{min}	K	300	298	290	300	250	100	700
T_{max}	K	500	800	305	390	600	700	2000

Fig. 9 shows the stability limits for pairs of the pure selenium phases listed in Table 2 according to reactions I-III, compared to the range of oxygen potentials for LWR UO_2 fuels estimated by Cordfunke and Konings[26]. The results indicate that at typical operation temperatures of 1500 K in the center of the fuel pellet, α-USe_2 would be the stable phase. As the SNF cools down (T < 700 K) metallic Se becomes more stable. Thus, during reactor operation formation of selenide is favoured, whereas under storage conditions there is a tendency for conversion to metallic Se.

Whether such a conversion can take place will largely depend on kinetic factors. If Se fission products are first stored as dispersed selenide ions in the matrix, as indicated by our results, a subsequent transformation to a discrete Se(0) phase in the fuel-cladding gap would require high ionic mobility. However, reaction and diffusion rates rapidly decrease as the fuel cools below 1000 K[26], thus hindering migration and oxidation of Se(-II) to Se(0).

According to Fig. 9, easily soluble oxidized forms like Se(IV) and Se(VI) should not be stable within the fuel matrix, neither under reactor operation nor under storage conditions. Preliminary calculations, to be presented in a separate paper, indicate that the formation of the $U(O_{2-y}Se_y)$ solid solution postulated to explain our X-ray spectroscopy results would even expand the Se(-II) stability region in Fig. 9.

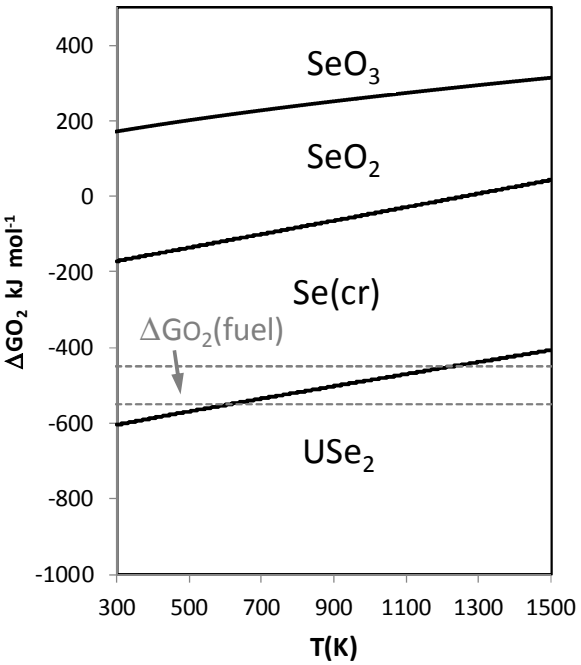

Fig. 9 Ellingham diagram showing the stability regions of the indicated selenium phases, compared with the range of oxygen potentials for LWR UO_2 fuels estimated by Cordfunke and Konings[26].

5. Conclusions

Our findings and arguments provide a mechanistic explanation of the results from SNF aqueous leaching experiments, which indicate no or insignificant release of Se[9]. The detection limit in those experiments implied that less than 0.22 % of the Se FP inventory was leached after about 100 days leaching time. Recent experiments with Swedish SNF[30], in which care was taken to reduce the detection limit of ICP analyses, indicate that 0.5%-0.8 % of the Se FP inventory is released to aqueous solution after 1 year leaching, demonstrating that only a tiny fraction of the FP inventory is leachable. Such percentages,

though still significant for safety assessment calculations, are much lower than the conservative values assumed in earlier safety assessments for ^{79}Se in high burnup fuel (up to 14 %)[8] based on the lack of reliable data and the limited understanding on Se chemistry in SNF.

In this contribution, we provide X-ray spectroscopic and thermodynamic evidence that a substantial fraction of the ^{79}Se is tightly bound to the fuel matrix via substitution of oxygen sites in the UO_2 lattice as reduced, sparingly soluble selenide ion. Our results explain why Se is much less soluble than I and Cs when SNF is leached in aqueous solutions and provide strong arguments to support the (still scarce) SNF leaching data indicating very weak fast Se release.

This result provides the necessary understanding to reduce conservatism in the choice of the corresponding IRF parameter in safety assessment calculations and therefore helps improving the reliability of such assessments.

Acknowledgements

The research leading to these results has received funding from the European Atomic Energy Community's Seventh Framework Programme (FP7/2007–2011) under Grant Agreement No. 295722, the FIRST-Nuclides project. It also benefited from financial support by the TALISMAN project (Transnational Access to Large Infrastructure for a Safe Management of ActiNide) under grant TALI-C03-10. Many thanks are due to Westinghouse and Krernkraftwerk Leibstadt AG for delivering the investigated samples and permission to publish these results. We are grateful to Prof. James Ibers (Northwestern University) for coordinating the synthesis and organizing the transport of the α-USe_2 sample to Switzerland.

Notes and references

‡ The observed intensity variation may be explained by thickness and boundary effects.

§ Each SNF spectrum in Fig. 5 is the average of several single spectra collected at different locations of the specified sample (RIM, CEN for Oskarshamn-III; 4 different samples from the same pellet for Leibstadt).

1 P.A. Witherspoon and G.S. Bodvarsson, Geological Challange in Radioactive Waste Isolation, Lawrence Berkeley National Laboratory, Berkeley (2006).
2 L.O. Werme, L.H. Johnson, V.M. Oversby, F. King, K. Spahiu, B. Grambow and D.W. Shoesmith (2004), Technical report TR-04-19, Svensk Kärnbränslehantering AB (SKB), Stockholm, Sweden.
3 L. Johnson, C. Ferry, Ch. Poinssot and P. Lovera, *J. Nucl. Mat.*, **346**, 2005, 56-65.
4 Ch. Poinssot, C. Ferry, P. Lovera, Ch. Jégou and J.-M. Gras, *J. Nucl. Mat.*, **346**, 2005, 66-77.
5 M. Jonsson, F. Nielsen, O. Roth, E. Ekeroth, S. Nilsson and M.M. Hossain, *Environ. Sci. Technol.*, **41**, 2007, 7087-7093.
6 M. Trummer and M. Jonsson, *J. Nucl. Mat.*, **396**, 2010, 163-169.
7 T.E. Eriksen, D.W. Shoesmith, M. Jonsson, *J. Nucl. Mat.*, **420**, 2012, 409-423.
8 D. Cui, J. Low and K. Spahiu, *Energy Env. Sci.*, **4**, 2011, 2537-2545.
9 L. Johnson, I. Günther-Leopold, J. Kobler Waldis, H.P. Linder, J. Low, D. Cui, E. Ekeroth, K. Spahiu and L.Z. Evins, *J. Nucl. Mat.*, **420**, 2012, 54–62.
10 D. Roudil, C. Jegou, V. Broudic, B. Muzeau, S. Peuget, X. Deschanels, *J. Nucl. Mater.*, **362**, 2007, 411–415.
11 F. Clarens, E. Gonzales-Robles, F.J. Gimenez, I. Casas, J. de Pablo, D. Serrano, D. Wegen, J.P. Glatz, A. Martinez-Esparza, Effect of burn-up and high burn-up structure on spent nuclear fuel alteration, Enresa Report 04, 2009.
12 D. Serrano-Purroy, F. Clarens, E. González-Robles, J.P. Glatz, D.H. Wegen, J. de Pablo, I. Casas, J. Giménez, A. Martínez-Esparza, *J. Nucl. Mater.*, **427**, 2012, 249–258.
13 A.C. Scheinost, R. Kirsch, D. Banerjee, A. Fernandez-Martinez, H. Zaenker, H. Funke and L. Charlet, *J. Cont. Hydrol.*, **102**, 2008, 228–245.
14 E. Curti , L. Aimoz and A. Kitamura, *J. Radioanal. Nucl. Chem.* **295**, 2013, 1655–1665.
15 L. Johnson, Ch. Poinssot, C. Ferry and P. Lovera. Estimates of the Instant Release Fraction for UO2 and MOX Fuel at t=0. Technical Report 04-08, Nagra, Wettingen, Switzerland, (2004).
16 E. Curti, A. Froideval-Zumbiehl, I. Günther-Leopold, M. Martin, A. Bullemer, H.P. Linder, C.N. Borca and D. Grolimund, *J. Nucl. Mat.*, **453**, 2014, 98-106.
17 T. Hermannsdörfer, P. Fischer, K. Mattenberger and O. Vogt, *J. Alloys and Compounds,* **414** , 2006, 14–19.
18 K. Mattenberger, L. Scherrer, O. Vogt, *J. Cryst. Growth,* **67** 1984, 467–471.
19 H.P. Beck and W. Dausch, *J. Solid State Chem.*, **80**, 1989, 32-39.
20 B. Ravel and M.J. Newville, *Synchrotron Rad.*, **12**, 2005, 537-541.
21 Y. Joly, *Phys. Rev. B*, **63**, 2001, 125120-1 –125120-10.
22 A. Belsky, M. Hellenbrandt, V.L. Karen, P. Luksch, *Acta Cryst. B*, **58** , 2002, 364–369.
23 Th.A. Carlson, C.W. Nestor Jr., Th. Tucker and F.B. Malik, *Phys. Rev.,* **169**(1), 1969, 27-36.
24 D.R. Olander, Fundamental Aspects of Nuclear Reactor Fuel Elements, National Technical Information Center, U.S. Dept. of Commerce, Springfield, 1976.
25 H. Kleykamp, *J. Nucl. Mat.* ***131***, 1985, 221-246.
26 E.H.P. Cordfunke and R.J.M. Konings, *J. Nucl. Mat.* ***152***, 1988, 301-309
27 Å. Olin, B. Nolang, L.O. Ohman, E. Osadchii, E. Rosen. In: F.J. Mompean, J. Perrone, M. Illemassene (eds.) Chemical Thermodynamics of Selenium. Chemical thermodynamics 7, OECD, Nuclear Energy Agency, Elsevier, Amsterdam, 2005.
28 R. Guillamont, Th. Fanghänel, V. Neck, J. Fuger, D.A. Palmer, I. Grenthe, M.H. Rand. In: : F.J. Mompean, M. Illemassene, C. Domenech-Orti, K. Ben Said (eds.) Update on the Chemical Thermodynamics of Uranium, Neptunium, Plutonium, Americium and Technetium. Chemical thermodynamics 5, OECD, Nuclear Energy Agency, Elsevier, Amsterdam, 2003.
29 NIST Web book, http: //webbook.nist.gov/cgi/cbook.cgi?ID=C7782447&Mask=1
30 A. Puranen, M. Granfors and O. Roth. In: FIRST-Nuclides Deliverable No. 5.4, Final (3rd) Annual Workshop Proceedings, European Commission, 167-172.